Electronic Supplementary Information (ESI)

Multi-interfacial Charge Polarization for Enhancing Hydrogen Evolution Reaction

Di Zhao, †,[a] Mengyun Hou, †,[a] Wuyi Feng,[a] Pengyu Song,[a] Kaian Sun,[b] Lirong Zheng,[c] Shoujie Liu,[b] Jiatao Zhang,*[a] Minhua Cao,*[a] Chen Chen*[b]*

[a]*Key Laboratory of Cluster Science, Ministry of Education of China, Beijing Key Laboratory of Photoelectronic/Electrophotonic Conversion Materials, School of Chemistry and Chemical Engineering, Beijing Institute of Technology, Beijing 100081, China*
[b]*Department of Chemistry, Tsinghua University, Beijing 100084 (China)*
[c]*Beijing Synchrotron Radiation Facility, Institute of High Energy Physics, Chinese Academy of Sciences, Beijing 100049, China*
† These authors contributed equally to this work.

Experimental Section

Preparation of MoP/ufMoS$_2$@NC NSs.

All chemicals used were analytical grade without further purification. Typically, the MoP/$_{uf}$MoS$_2$@NC NSs were synthesized as follows. First, 0.143 mmol of amountammonium molybdate tetrahydrate [$(NH_4)_6Mo_7O_{24}{\cdot}4H_2O$)] , 1 mmol $(NH_4)_2HPO_4$ and 1.5 mmol thiourea were dispersed in 15 mL of deionized water to form transparent solution under vigorous stirring. Then, 1.0 g of F127 was added into the mixture solution under vigorous stirring. Subsequently, the mixture was subjected to freeze-drying for 24 h to yield a precursor. Finally, the typical sample MoP/$_{uf}$MoS$_2$@NC can be obtained by calcining the precursor at 750 ℃ for 3 h in H_2/Ar atmosphere. In order to investigate the role of the constructed interfaces in electrochemical HER, control samples were prepared according to Table S1. The obtained products were denoted as sample MoP/$_{uf}$MoS$_2$@NC-x, where x represented the addition amount (mmol) of thiourea. In addition, the control samples of bare MoP (MoP), bare MoS_2 (MoS_2), the hybrid of MoP and MoS_2 (MoP/MoS_2) without carbon coating, and the composite comprising of MoP/MoS_2 nanoparticles and carbon (MoP/$_{uf}$MoS$_2$@NC-phy) were also synthesized by physically mixing according to Table S1.

Characterizations.

Powder XRD datum were acquired on a D8 Advance (Super speed) XRD diffractometer (Bruker). The general size and morphology of the products were characterized by a field-emission scanning electron microscope (SEM, Hitachi S-4800). Transmission electron microscopy (TEM) and high-resolution transmission electron microscopy (HRTEM) were carried on a H-8100 transmission electron microscope operating at a 200 kV accelerating voltage. The X-ray photoelectron spectroscopy (XPS) experiments were tested on the ESCALAB 250 spectrometer (Perkin-Elmer). The Brunauer-Emmett-Teller (BET) specific surface areas of typical products were performed at 77 K in a Belsorp-max surface area detecting instrument.

Electrochemical Measurements for hydrogen evolution reaction.

All the electrochemical measurements were conducted using a CHI760E potentiostat (CH Instruments, China) in a typical three-electrode setup with an hydrogen-saturated electrolyte solution of 0.5 M H_2SO_4 (pH = 0.3): a graphite rod as the counter electrode, a saturated calomel electrode (SCE) as the reference electrode and the working electrode was a glassy carbon (3 mm in diameter) supporting the measured materials. Catalyst ink was prepared by dispersing 2

mg of catalyst into 450 μL of ethanol solvent containing 50 μL of 5 wt% Nafion and sonicated for 30 min. Then 10 μL of the catalyst ink (containing 40 μg of catalyst) was loaded onto a glassy carbon with a loading of ca. 0.57 mg cm^{-2}) after air-drying. For comparison, the commercial 20 wt % Pt/C was supported on the glassy carbon with the same loading. In all measurements, the SCE reference electrode was calibrated with respect to reversible hydrogen electrode (RHE). LSV was conducted in 0.5 M H_2SO_4 and 1 M KOH solutions with a scan rate of 10 mV s^{-1}. The time dependency of catalytic currents during electrolysis for the catalyst was tested in 0.5 M H_2SO_4 and 1 M KOH at 10 mV cm^{-2}. Electrochemical impedance spectroscopy (EIS) measurements were also carried out in the frequency range of 100 kHz–0.01 Hz. The potentials in the final graphs were converted to the potentials versus the reversible hydrogen electrode (RHE) according to the following calculation: E (RHE) = E (SCE) + 0.241 + 0.0592 pH. The effective electrochemically active surface area (ECSA) was measured by cyclic voltammetry (CV) using the same working electrodes at a potential window of 0.29-0.383 (RHE). CV curves were obtained at different scan rates of 10, 20, 30, 40, 50, 60, 70, 80, 120, 160 mV s^{-1}. After plotting charging current density differences ($\Delta j = j_a - j_c$ at the overpotential of 340 mV) versus the scan rates, the slope, twice of the double-layer capacitance C_{dl}, is used to represent ECSA. We used phosphate acid (H_3PO_4: 0.5 M and 1 M H_3PO_4 solutions) to block the possible py-N ctive sites.

XAFS measurements.

The X-ray absorption find structure spectra (Mo K-edge) were collected at 1W1B station in Beijing Synchrotron Radiation Facility (BSRF). The storage rings of BSRF was operated at 2.5 GeV with an average current of 250 mA. Using Si(111) double-crystal monochromator, the data collection were carried out in transmission/fluorescence mode using ionization chamber. All spectra were collected in ambient conditions.

XAFS Analysis and Results.

The acquired EXAFS data were processed according to[1] the standard procedures using the ATHENA module implemented in the IFEFFIT software packages[1-2]. The k^3-weighted EXAFS spectra were obtained by subtracting the post-edge background from the overall absorption and then normalizing with respect to the edge-jump step[3]. Subsequently, k^3-weighted $\chi(k)$ data of Fe K-edge were Fourier transformed to real (R) space using a hanning windows (d_k=1.0 $Å^{-1}$) to separate the EXAFS contributions from different coordination shells. To obtain the quantitative structural parameters around central atoms, least-squares curve parameter fitting was performed using the ARTEMIS module of IFEFFIT software packages.

Computational details.

A series of density functional theory (DFT) calculations were all done with the Vienna Ab initio Simulation Package (VASP) [4]. The electron-ion interaction was described using the projector augmented wave (PAW)[5], and the kinetic energy cutoff for plane wave expansions was set to 450 eV. The electron exchange and correlation energies were treated within a generalized gradient approximation (GGA) in the Perdew-Burke-Ernzerhof (PBE) exchange-correlation[6]. A DFT-D3 scheme of dispersion correction was used to describe the van der Waals (vdW) interactions in molecule adsorption[7]. The Brillouin zone was sampled using the Monkhorst-Pack 3×3×1 sampling[8] and the convergence criteria were 1×10^{-6} eV and 1×10^{-7} eV energy differences for solving for the electronic wave function in structure optimization and vibrational frequency calculations, respectively, and force convergence criterion of -0.02 eV $Å^{-1}$. To avoid the interactions between two adjacent periodic images, the vacuum thickness was set to be 15 Å. The electron smearing width of $\sigma = 0.05$ eV was employed according to the Methfessel-Paxton technique. The free energy correction was obtained similarly by including the zero-point energy (ZPE) and entropic contributions from vibrational degrees of freedom calculated with the substrate fixed, and the value gained by using Vaspkit.1.2.5[9].

The construction of the model is described as follows:

According to our previous work[10], the thermodynamically stable plane (001) in MoP and Mo atoms are exposed on the surface. It can be seen from the TEM images that the plane (100) of MoP forms a heterojunction with the plane (002) of MoS_2.

MoP: A 2x3 supercell consisting of 24 atoms from a MoP conventional cell of the lattice parameters of a=5.62 Å, b=3.24 Å, c=3.20 Å and α=β=90°, γ=90° was used firstly, then cleaving surface of plane (001) and the fractional thickness set to 2.0, adding vacuum thickness to build vacuum slab crystal of the lattice parameters of a=11.24 Å, b=9.73 Å, c=25.00 Å and α=β=γ=90°.

MoP_NC: A 3x3 supercell consisting of 36 atoms from a MoP conventional cell of the lattice parameters of a=5.62 Å, b=3.24 Å, c=3.20 Å and α=β=90°, γ=90° was used firstly, then cleaving surface of plane (001) and the fractional thickness set to 2.0 to get the MoP-layer.

A 4x4 supercell consisting of 64 carbon atoms from a graphene conventional cell of the lattice parameters of a=4.26Å, b=2.46Å and α=β=90°, γ=90° was used firstly, then deleted two connected carbon atoms for formed a defect, and C atoms were substituted by four N atoms in the innermost layer at the defect. Next, cleaving surface of plane (001) and the fractional thickness set to 1.0 to get the graphene-layer.

And then the MoP-layer matched graphene-layer to each other to construct a heterojunction, with the distance of two layers is 2.5 Å and choosing the average lattice parameter to build the new slab crystal of a=16.95 Å, b=9.79 Å, c=25 Å and α=β=90°, γ=90°. The lattice constant a mismatch degree are 0.53% of MoP-layer and 0.53% of graphene-layer.

MoPS_NC: A MoP conventional cell of the lattice parameters of a=5.62Å, b=3.24Å, c=3.20 Å and α=β=90°, γ=90° was used firstly, then cleaving surface of plane (100) and regulating the Mo-terminated of top and bottom surface with consisting of 5 atoms. Next a 5x1 super surface consisting of 25 atoms with the lengths u=16.22 Å, v=3.20 Å was built as the MoP'-layer.

A MoS_2 conventional cell of the lattice parameters of a=5.48 Å, b=3.17 Å, c=18.41 Å and α=β=90°, γ=90° was used firstly, then cleaving surface of plane (001) and regulating the S-terminated of top and bottom surface with consisting of 6 atoms. Next a 3x1 super surface consisting of 18 atoms with the lengths u=16.45 Å, v=3.17 Å was built as the MoS_2-layer.

And then the MoP'-layer matched graphene-layer to each other to construct a heterojunction, with the distance of two layers is 3.0 Å and choosing the average lattice parameter to build the new slab crystal of a=16.34Å, b=3.18Å, c=14.76 Å and α=β=90°, γ=90° as MoPS. The lattice constant a mismatch degree are 0.74% of MoP'-layer and 0.67% of MoS_2-layer.

Next, cleaving the surface of plane (0 1 0) of MoPS and the fractional thickness set to 2.0 to get the MoPS-layer with the lengths of u=14.76 Å, v=16.34 Å.

A graphene conventional cell of the lattice parameters of a=2.46Å, b=4.26Å and α=β=90°, γ=90° was used firstly, then cleaving surface of plane (001) with consisting of 4 atoms. Next a 6x4 super surface consisting of 96 atoms with the lengths u=14.76 Å, v=17.04 Å was built, then deleted two connected carbon atoms for formed a defect, and C atoms were substituted by four N atoms in the innermost layer at the defect as graphene'-layer.

And then the MoPS-layer matched graphene'-layer to each other to construct a heterojunction, with the distance of two layers is 2.5 Å and choosing the average lattice parameter to build the new slab crystal of a=14.76Å, b=16.69Å, c=25.00 Å and α=β=90°, γ=90° as MoPS_NC. The lattice constant b mismatch degree are 2.14% of MoPS-layer and 2.05% of graphene'-layer.

The adsorption energy was calculated by subtracting the energies of the isolated adsorbate and the catalyst from the total energy of the adsorbed system:

E_b = E (slab + adsorbate) - E (slab) - E (adsorbate)

The pathway by which the HER occurs under base condition are generally reported to proceed according to the following step:

$H^+ + e^- + * \rightarrow *H$

$*H \rightarrow * + 1/2\ H_2$

Where the * refers to the catalytic, and the *one refers to the species that adsorbed on the activity sites.

The kinetic energy barrier of the initial water dissociation step (ΔG_H2O) is applied as an activity descriptor for HER under alkaline condition, which can be calculated as follows:

ΔG_H_2O = G_TS – G_IS

where G_TS and G_IS are the free energy of the transient state and the initial state for water dissociation, respectively.

Neglect PV contribution to translation for adsorbed molecules, the free energy of every step was calculated according to the equation of $G = E + H_{cor} - TS = E + G_{cor}$, where E is the energy of every specie obtained from DFT calculations, and S are entropy, while T is 298.15 K. The H_{cor} and G_{cor} are the thermal correction to enthalpy and the thermal correction to Gibbs free energy, respectively. The G_{cor} of *H and $*H_2O$ were taken from the frequency DFT calculation and got value by using Vaspkit.1.2.5.

The Gibbs free energy of the proton-electron pairs ($H^+ + e^-$) related in the PECT progress[11], whereas the fact that the proton-electron pairs is in equilibrium with gaseous H_2 at 0 V versus standard hydrogen electrode (U = 0, pH = 0, and pressure = 1 bar, and temperature = 298.15K):

$\mu(H^+ + e^-) = 1/2\ \mu(H_2\ (g))$

According to Vaspkit.1.2.5, the internal energy of gas molecular gained from the formula: U(T) = ZPE + ΔU(0-T), the enthalpy of gas molecular gained from the formula: H(T) = U(T) + PV = ZPE + ΔU(0-T) + PV, and the Gibbs free energy of gas molecular gained from the formula: $G(T) = H(T) - TS = ZPE + \Delta U(0\text{-}T) + PV - TS = E\_DFT + G_{cor}'$.

Where E_DFT is the energy of the free gas molecule obtained from DFT calculations, G_{cor}' is the thermal correction to Gibbs free energy of the free gas molecule obtained from the frequency DFT calculation and got value by using Vaspkit.1.2.5, with the temperature of 298.15K, the pressure of H_2O and H_2 were 0.035 atm and 1 atm, respectively, and all species input 1 as the value of spin multiplicity.

The d-band center[12] of the 4d orbitals of Mo obtained from their PDOS by using equation:

$$\varepsilon_d = \frac{\int_{-\infty}^{+\infty} \varepsilon f(\varepsilon) d\varepsilon}{\int_{-\infty}^{+\infty} f(\varepsilon) d\varepsilon}$$

where, the f(ε) is the PDOS of an energy level of ε.

The charge density difference was evaluated using the formula $\Delta\rho = \rho(\text{Mo/substrate}) - \rho(\text{Mo}) - \rho(\text{substrate})$, then analyzed by using the VESTA code[13].

Supporting Figure and Tables

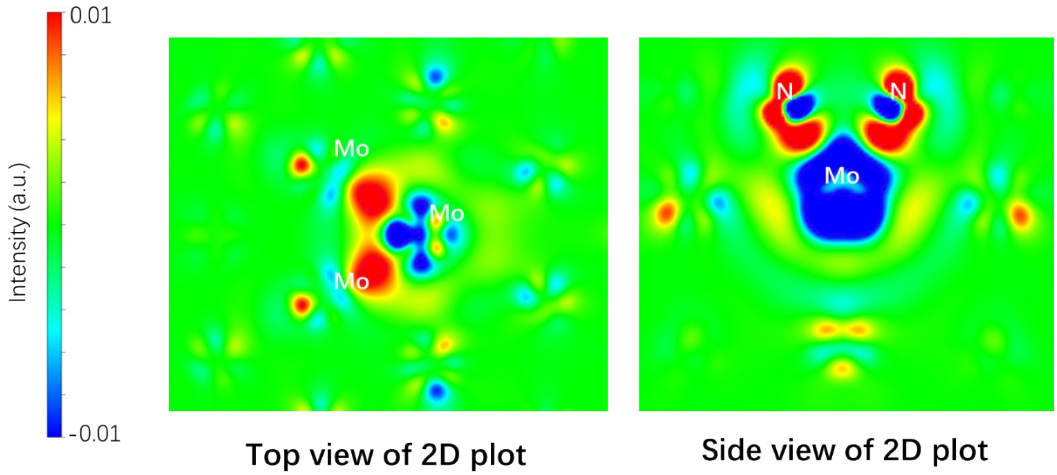

Figure S1. Multiple views of charge density differences of MoP@NC. The isosurface level set to 0.005 eÅ^{-3}, where charge depletion and accumulation were depicted by red and purple, respectively.

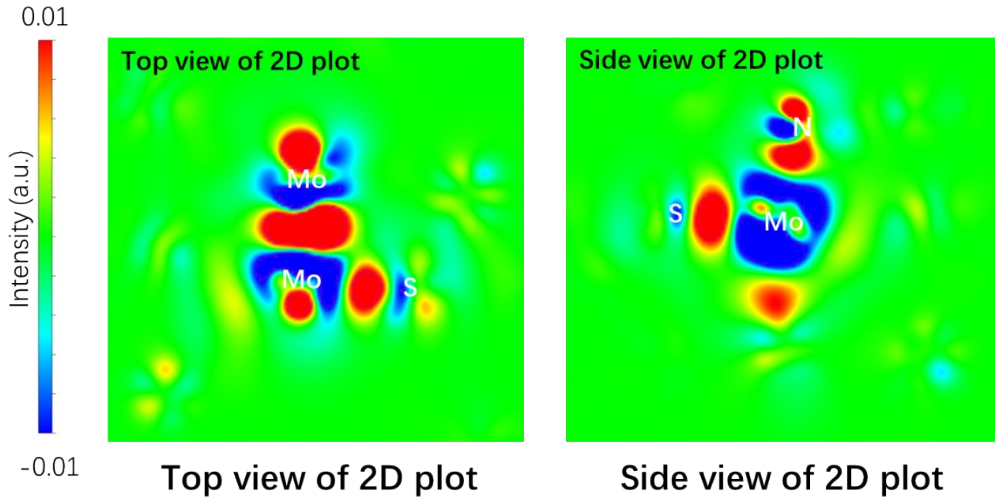

Figure S2. Multiple views of charge density differences of MoP/$_{uf}$MoS$_2$@NC. The isosurface level set to 0.005 eÅ-3, where charge depletion and accumulation were depicted by red and purple, respectively.

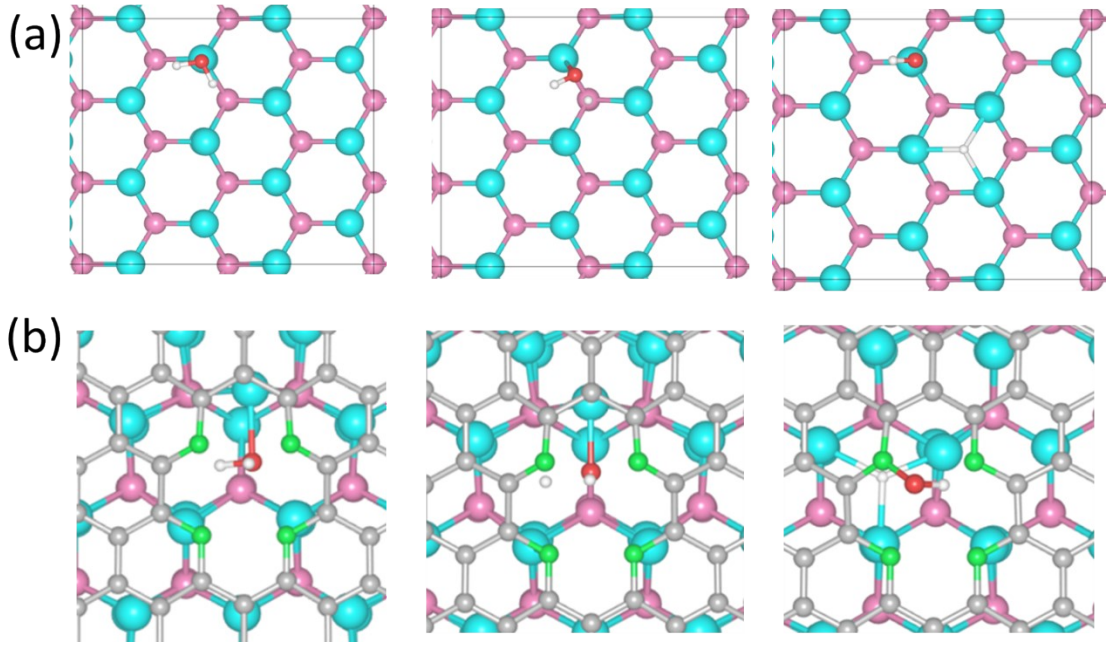

Figure S3. Diagrams of Volmer step with initial state (IS), transition state (TS) and finial state (FS) of (a) MoP and (b) MoP@NC, respectively.

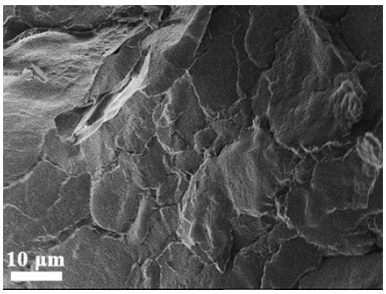

Figure S4. SEM image of as-synthesized precursor for pomegranate-like MoP/$_{uf}$MoS$_2$@NC.

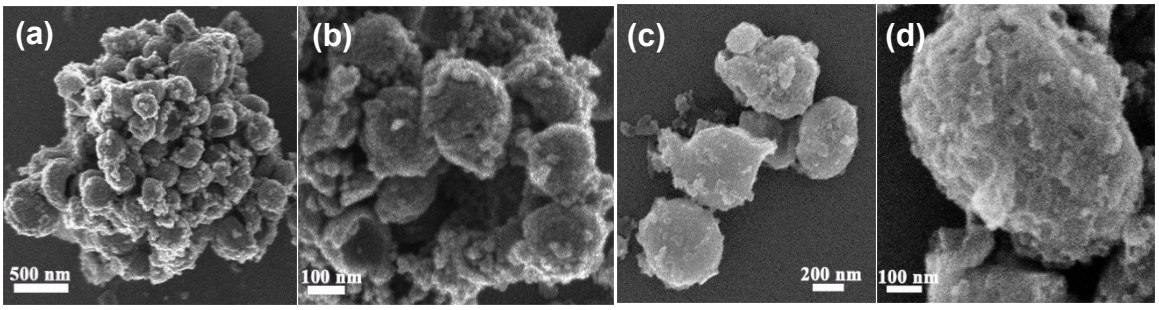

Figure S5. (a,b) Low- and (c,d) High-magnification SEM images of MoP/$_{uf}$MoS$_2$@NC.

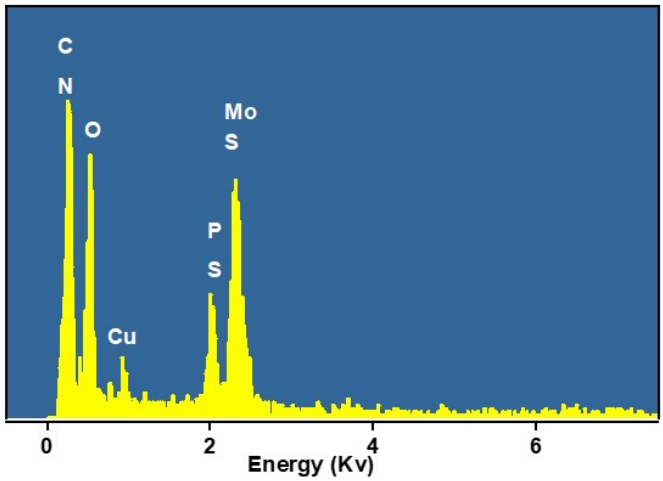

Figure S6. EDS recorded on an individual MoP/$_{uf}$MoS$_2$@NC.

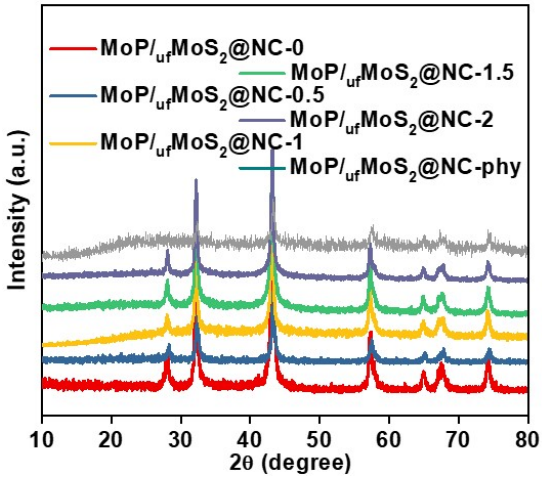

Figure S7. XRD patterns of the all control samples for MoP/$_{uf}$MoS$_2$@NC-X and MoP/$_{uf}$MoS$_2$@NC-phy.

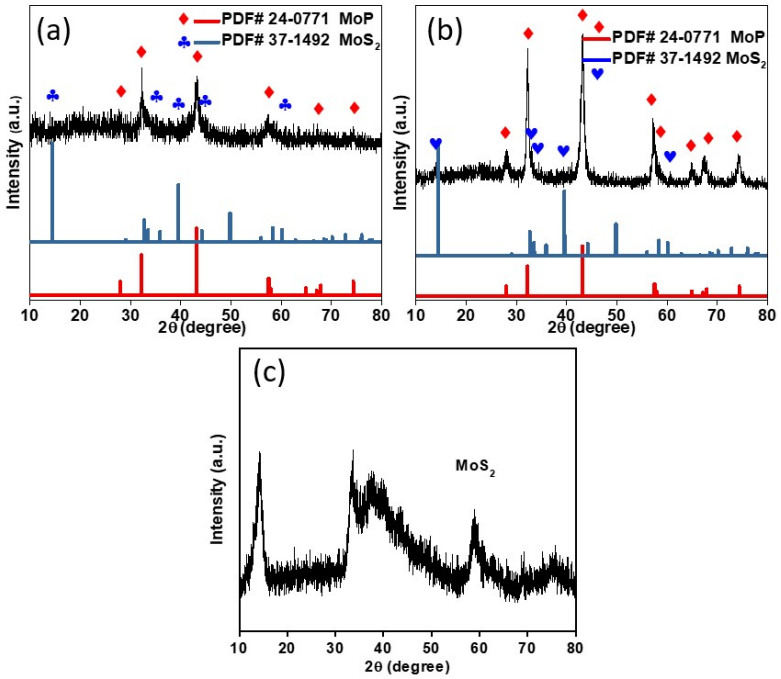

Figure S8. XRD patterns of the control samples for MoP/$_{uf}$MoS$_2$@NC-4, MoP/MoS$_2$ and MoS$_2$.

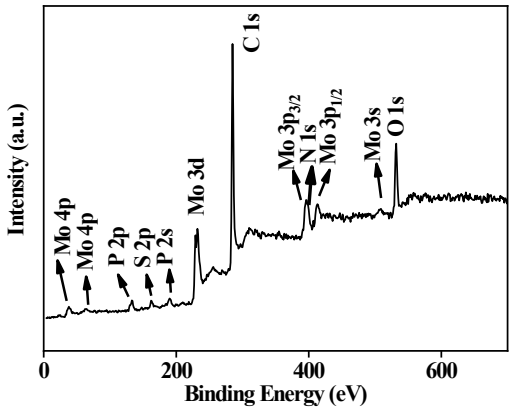

Figure S9. XPS survey spectrum of MoP/$_{uf}$MoS$_2$@NC.

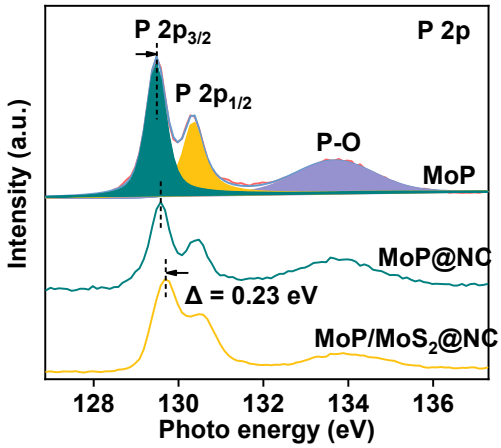

Figure S10. High-resolution P 2p XPS spectra of MoP/$_{uf}$MoS$_2$@NC, MoP@NC, and bulk MoP.

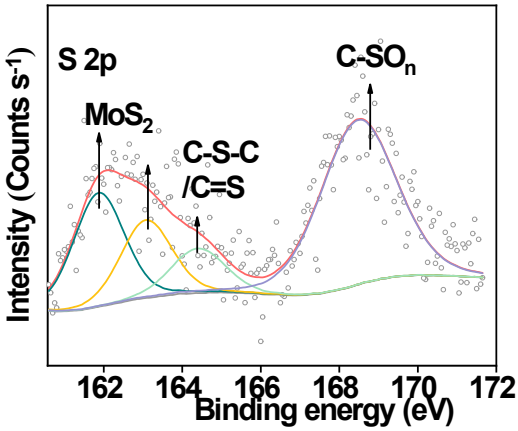

Figure S11. High-resolution S 2p XPS spectra of MoP/$_{uf}$MoS$_2$@NC. Figure S11 shows the S 2p spectrum. The main doublet located at binding energies of 161.9 and 163.3 eV, corresponds to the S 2p$_{3/2}$ and S 2p$_{1/2}$ lines of MoS$_2$.[14] Another two peaks centered at 164.7 and 168.8 eV, indicating the presence of sulfur in two forms which are attributed to the sulfur binding in -C-S-/-C=S- bonds and the oxidized sulfur (-C-SO$_n$-C-).[15]

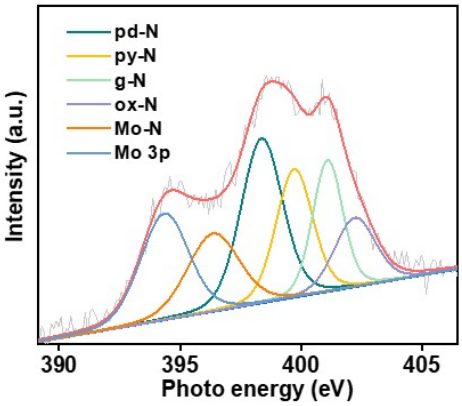

Figure S12. High-resolution N 1s XPS spectra of MoP/$_{uf}$MoS$_2$@NC. The N 1s XPS spectrum was deconvoluted into four peaks of pyridinic N (py-N), pyrolic N (py-N), graphitic N (g-N) and oxidized nitrogen (ox-N) at the binding energies of around 398.4, 399.7, 401.1 eV and 402.2, respectively (Figure 3c).[16]

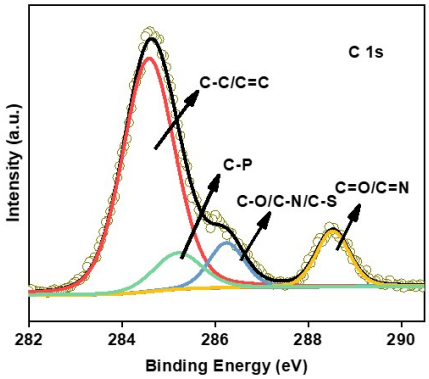

Figure S13. High-resolution C 1s XPS spectra of MoP/$_{uf}$MoS$_2$@NC. The deconvolution of C1s XPS spectra (Figure S11) yielded for major components, corresponding to C-C/C=C (284.7 eV), C-P (285.2 eV), C–N/C–O/C–S (286 eV) and C=O/C=N (288.6 eV).[17]

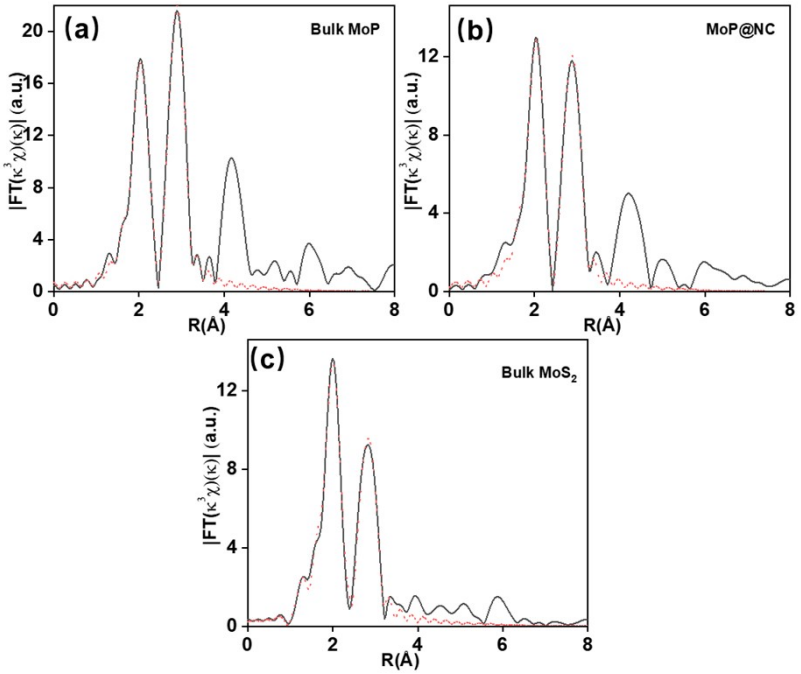

Figure S14. k The EXAFS fitting for MoP, MoS_2 and MoP@NC.

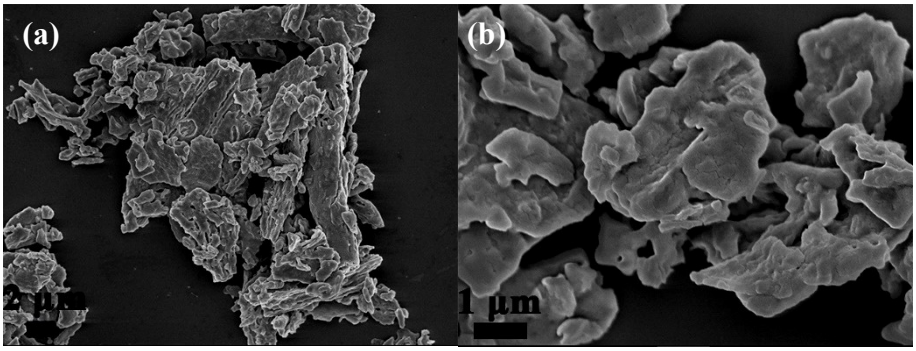

Figure S15. SEM images of MoP/$_{uf}$$MoS_2$ NPs.

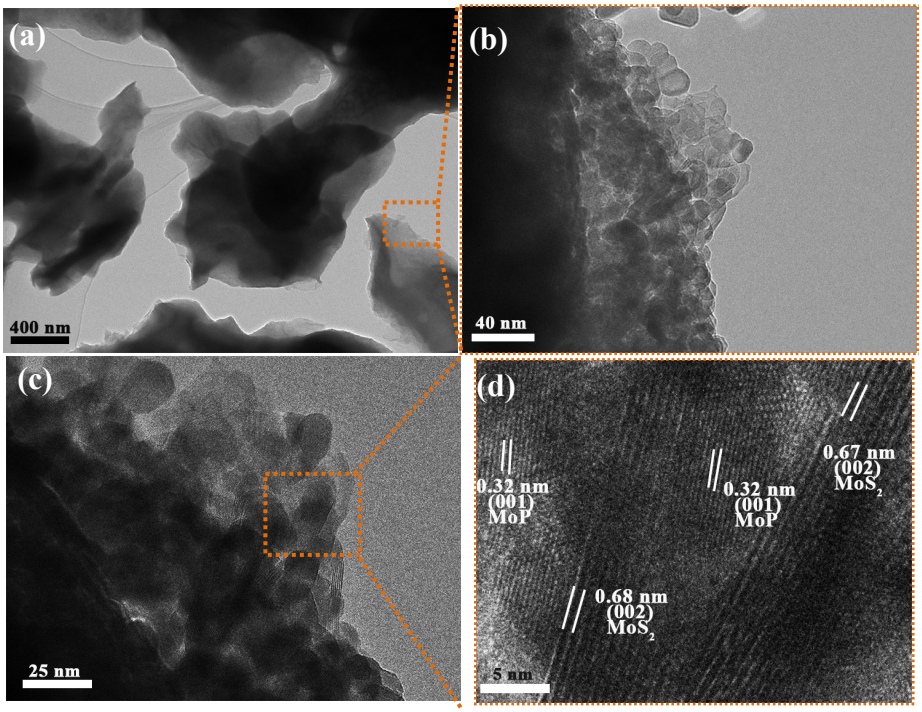

Figure S16. TEM images of MoP/$_{uf}$MoS$_2$ NPs.

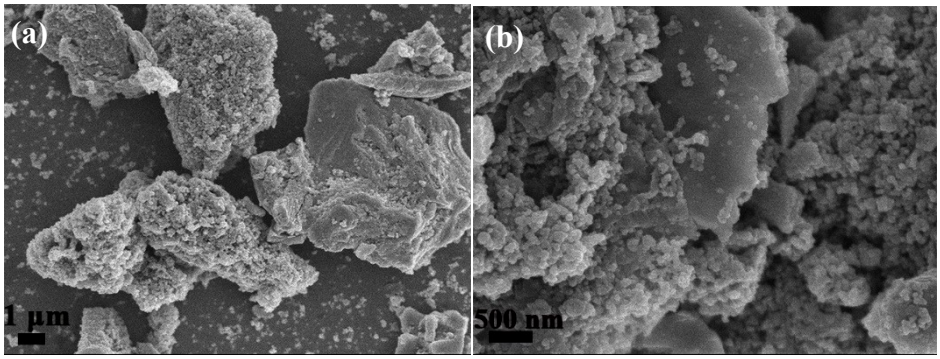

Figure S17. SEM images of MoP/$_{uf}$MoS$_2$@NC-phy.

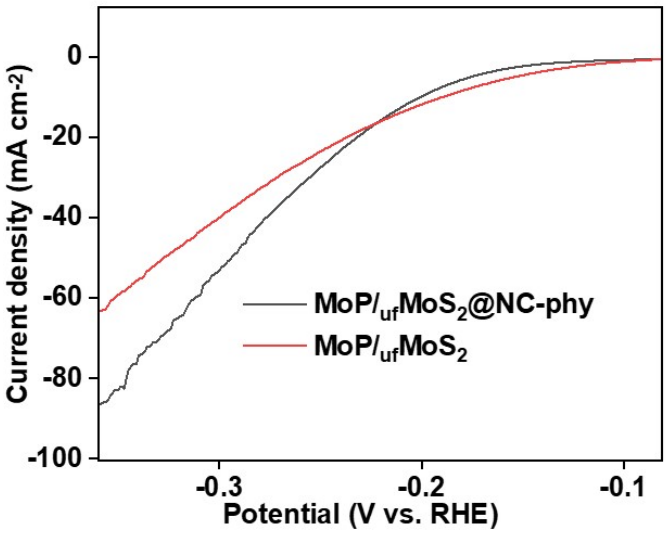

Figure S18. Polarization curves of MoP/$_{uf}$MoS$_2$@NC-phy and MoP/$_{uf}$MoS$_2$ nanoparticles in 0.5 M H_2SO_4 at a scan rate of 10 mV s^{-1}.

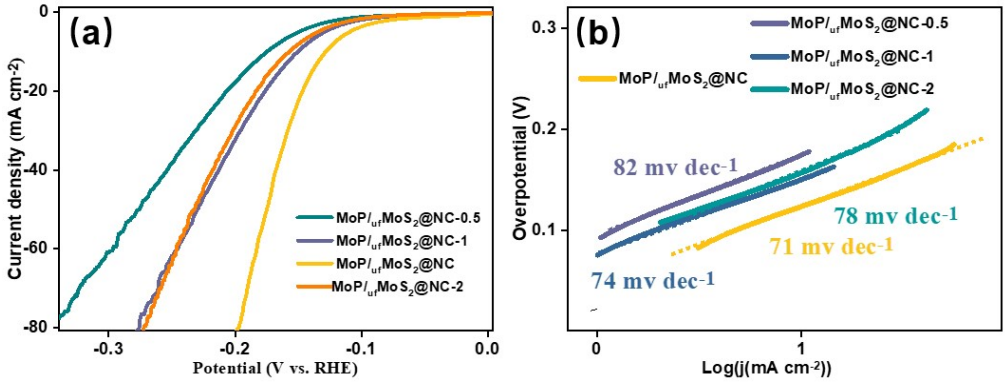

Figure S19. Polarization curves and their corresponding Tafel plots of MoP/$_{uf}$MoS$_2$@NC-x with different MoS$_2$ decorating in 0.5 M H_2SO_4 at a scan rate of 10 mV s^{-1}.

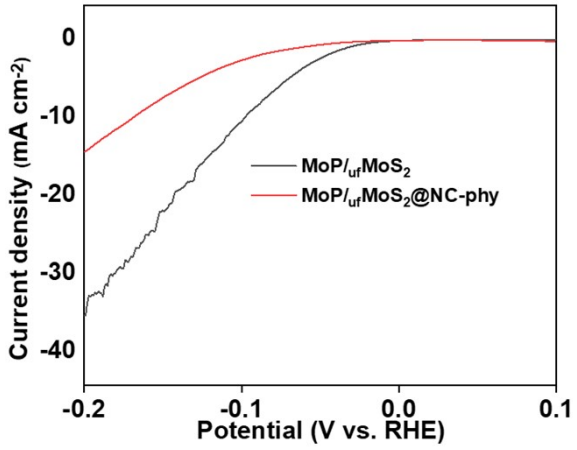

Figure S20. Polarization curves of MoP/$_{uf}$MoS$_2$@NC-phy and MoP/$_{uf}$MoS$_2$ nanoparticles in 1 M KOH at a scan rate of 10 mV s^{-1}.

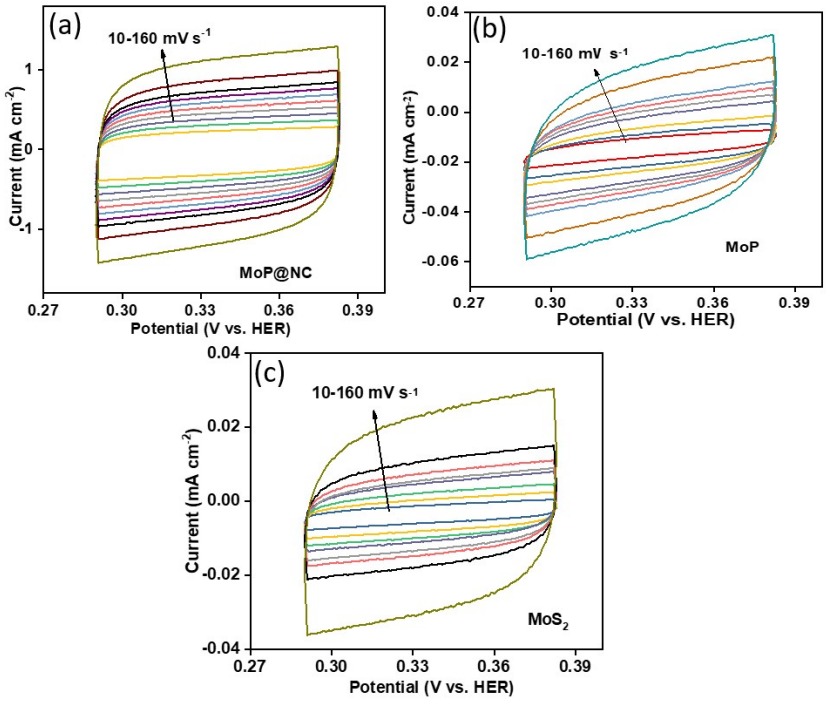

Figure S21. Cyclic voltammograms (CVs) of MoP@NC NSs, MoP and MoS_2 control samples where no Faradaic processes measured at different scan rates from 10 to 160 mV s^{-1} in the potential range of 0.29-0.383 V.

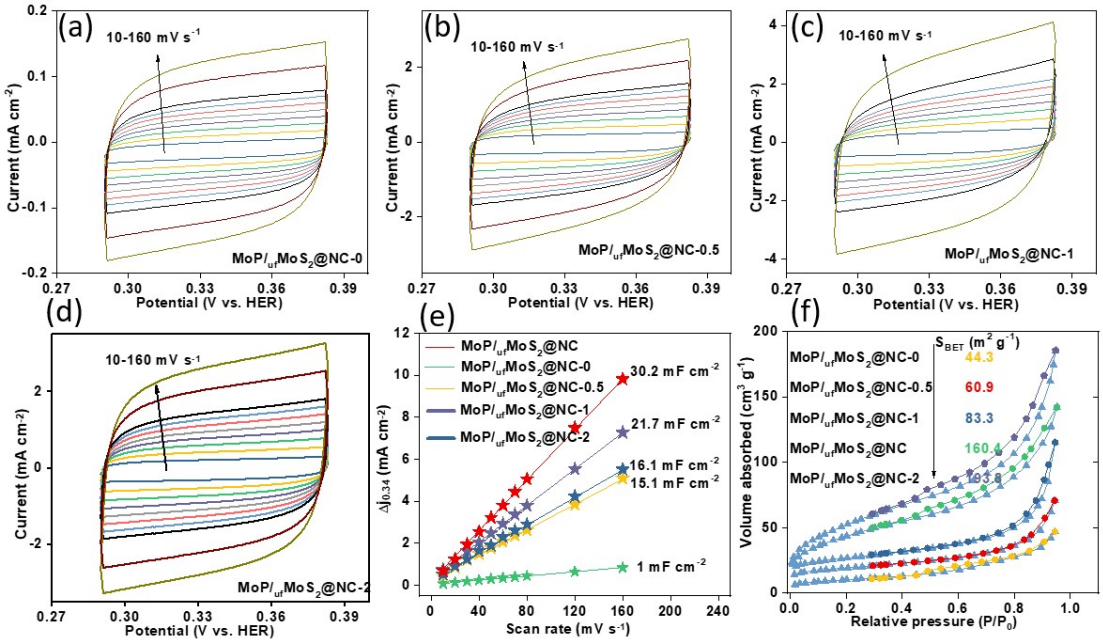

Figure S22. (a-d) Cyclic voltammograms (CVs) of $MoP/_{uf}MoS_2$@NC-X (x= 0, 0.5, 1 and 2) samples measured at different scan rates from 10 to 160 mV s^{-1} in the potential range of 0.29-0.383 V. (c) Charging current density differences plotted against scan rates. The linear slope, equivalent to twice the double-layer capacitance, Cdl, was used to represent the ECSA. (f) N_2 adsorption and desorption curves of all $MoP/_{uf}MoS_2$@NC-X samples and corresponding BET surface areas.

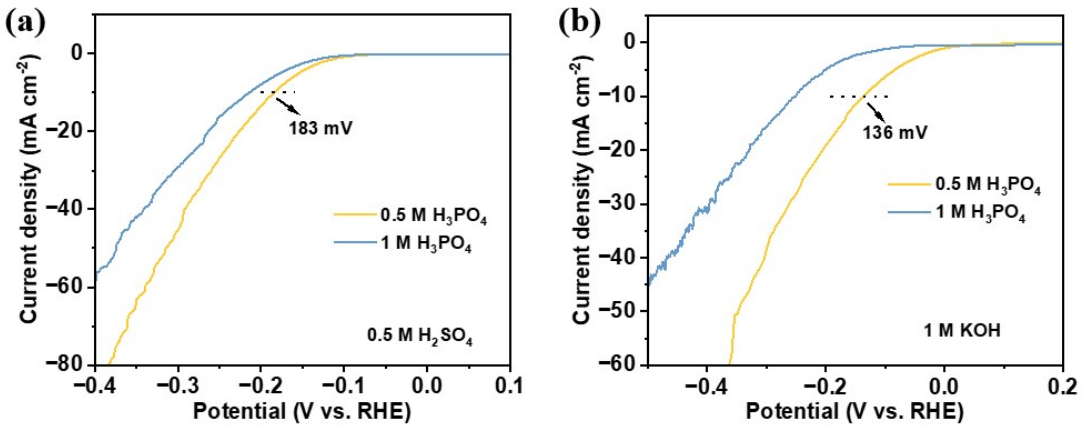

Figure S23. LSV curves of MoP/$_{uf}$MoS$_2$@NC (soaking in 0.5, 1 M H_3PO_4 solutions) in 0.5 M H_2SO_4 and 1 M KOH electrolyte.

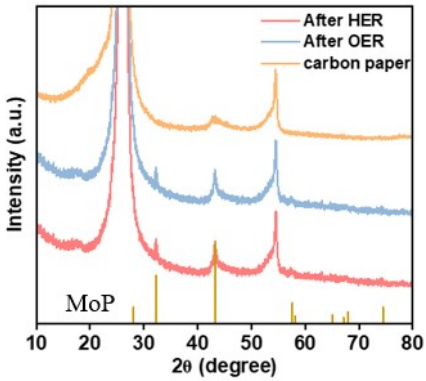

Figure S24. XRD characterization of MoP/$_{uf}$MoS$_2$@NC catalyst after a long time stability testing.

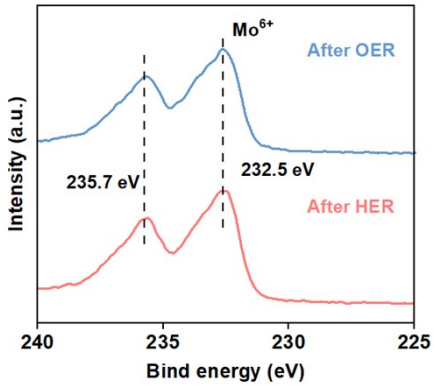

Figure S25. XPS spectra of Mo 3d for MoP/$_{uf}$MoS$_2$@NC before and after HER and OER stability test.

Table S1. Different reaction conditions for the synthesis of MoP/$_{uf}$MoS$_2$@NC and other control samples.

Samples	$(NH_4)_6Mo_7O_{24}.4H_2O$) [mmol]	$(NH_4)_2HPO_4$ [mmol]	F127 [g]	Thiourea [mmol]	Urea [mmol]
MoP/$_{uf}$MoS$_2$@NC	0.143	1	1	1.5	-
MoP@NC	0.143	1	1	-	1.5
MoP	0.143	1	0	0	-
MoS$_2$	0.143	0	0	1.5	-
MoP/$_{uf}$MoS$_2$@NC-0	0.143	1	1	0	-
MoP/$_{uf}$MoS$_2$@NC-0.5	0.143	1	1	0.5	-
MoP/$_{uf}$MoS$_2$@NC-1	0.143	1	1	1	-
MoP/$_{uf}$MoS$_2$@NC -2	0.143	1	1	2	-
MoP/$_{uf}$MoS$_2$@NC-4	0.143	1	1	4	-
MoP/MoS$_2$	0.143	1	0	1.5	-
NC	-	-	1	-	1.5
MoP/$_{uf}$MoS$_2$@NC - phy	0.143	1	1	1.5	-

Table S2. Local structure parameters around Mo estimated by EXAFS analysis

	Shell	N[a]	R (Å) [b]	σ^2 (Å$^2\cdot10^{-3}$) [c]	ΔE_0 (eV)[d]	*R* factor (%)
Bulk MoP	Mo-P	6.1	2.45	3.5	2.8	0.2
	Mo-Mo	8.0	3.21	4.1	1.7	
MoP@NC	Mo-P	5.2	2.45	4.0	3.0	0.2
	Mo-Mo	5.4	3.21	4.5	1.9	
MoP/$_{uf}$MoS$_2$@NC	Mo-P	4.8	2.45	4.5	2.4	0.3
	Mo-Mo	4.5	3.21	4.7	1.3	
Bulk MoS$_2$	Mo-S	4.2	2.42	3.6	1.2	0.7
	Mo-Mo	2.6	3.16	3.3	1.4	

[a]*N*: coordination numbers; [b]*R*: bond distance; [c]σ^2: Debye-Waller factors; [d]ΔE_0: the inner potential correction. *R* factor: goodness of fit. *S*02 were set as 0.90/0.96 for Mo-P/Mo-Mo, which was obtained from the experimental EXAFS fit of reference MoP by fixing CN as the known crystallographic value and was fixed to all the samples.

Table S3. Electrochemical parameters for MoP/$_{uf}$MoS$_2$@NSPC NSs and other control samples.

Samples	Catalysis condition	η_{10} [mV vs. RHE]	Tafel slope [mV dec^{-1}]	j_0 [mA cm^{-2}]
MoP/MoS$_2$@NSPC	**0.5 M H_2SO_4**	**120**	**71**	**0.240**
	1 M KOH	**80**	**62**	**0.537**
MoP@NC	0.5 M H_2SO_4	235	80	0.017
	1 M KOH	230	73	0.028
MoP	0.5 M H_2SO_4	350	107	0.016
	1 M KOH	280	109	0.032
MoS$_2$	0.5 M H_2SO_4	500	154	0.007
	1 M KOH	320	168	0.102
Pt/C (20%)	0.5 M H_2SO_4	42	32	0.251
	1 M KOH	45	53	1.272

Table S4. Comparison of HER performance in acid and alkaline solutions for MoP/$_{uf}$MoS$_2$@NC and other MoP-based electrocatalysts.

Catalyst	**Working electrode**	**Catalysis condition**	**Loading amount [mg cm^{-2}]**	**η_{10} [mV vs. RHE]**	**j_0 [mA cm^{-2}]**	**Tafel slope [mV dec^{-1}]**	**Ref.**
MoP/$_{uf}$MoS$_2$@NC	Glassy carbon	0.5 M H_2SO_4 1 M KOH	0.57 0.57	120 80	0.240 0.537	71 62	This work
MoP NW/CC	Carbon cloth	0.5 M H_2SO_4 1 M KOH	2 2	113 103	/ /	53.3 65.6	[18]
MoP/NC	Glassy carbon	0.5 M H_2SO_4 1 M KOH	0.255 0.255	183 213	/ /	56.9 61	[19]
MoP nanoparticles	Glassy carbon	0.5 M H_2SO_4 1 M KOH	0.86 0.86	150 140	0.034 0.046	54 48	[20]
MoP@NCHSs-900	Glassy carbon	0.5 M H_2SO_4 1 M KOH	0.4 0.4	92	0.21	62	[10]
Porous MoP Nano-Octahedrons	Glassy carbon	0.5 M H_2SO_4 1 M KOH	0.41 0.41	153 180	0.21 /	66 78	[21]
MoP/CNT	Carbon fiber paper	0.5 M H_2SO_4 1 M KOH	0.5 0.5	83 86	0.416 0.965	60 73	[22]
MoP cluster	Glassy carbon	0.5 M H_2SO_4 1 M KOH	0.337 0.337	119 140	0.178 0.578	58 72	[23]
MoP	Glassy carbon	0.5 M H_2SO_4 1 M KOH	0.071 /	246 /	0.042 /	60 /	[24]
MoP microparticles	Glassy carbon	0.5 M H_2SO_4 1 M KOH	0.1 0.1	150 190	0.01 /	50 /	[25]

MoP-graphite nanomaterials	Glassy carbon	0.5 M H_2SO_4 1 M KOH	2 2	115 80	0.18 /	65 59	[26]
MoP/graphene oxide	Glassy carbon	0.5 M H_2SO_4 1 M KOH	1.6 1.6	236 162	/ 0.187	111 57	[27]
Closely interconnected network of MoP nanoparticles	Glassy carbon	0.5 M H_2SO_4 1 M KOH	0.36 /	125 /	0.086 /	54 /	[28]
MoS_2@MoP	Glassy carbon	0.5 M H_2SO_4 1 M KOH	0.35 0.35	108 119	/ /	76 85	[29]
MoS_2-MoP/FPC-3	Glassy carbon	0.5 M H_2SO_4 1 M KOH	/ /	144 /	/ /	41 /	[30]
$MoS_{2(1-x)}P_x$ Solid Solution	Glassy carbon	0.5 M H_2SO_4 1 M KOH	0.29 /	150 /	/ /	50 /	[31]
MoP_2 NPs/Mo	Metal Mo plate	0.5 M H_2SO_4 1 M KOH	/ /	143 194	0.06 /	57 80	[32]
N@$MoPC_x$ nanosheet	Glassy carbon	0.5 M H_2SO_4 1 M KOH	0.14 0.14	108 139	0.3424 0.3023	69.4 86.6	[33]
MoP-G-60-11	Glassy carbon		0.64	277	0.064	63	[34]

Supplementary references:

[1] B. Ravel, M. Newville, *J Synchrotron Radiat* **2005**, *12*, 537-541.

[2] D. C. Koningsberger, R. Prins, **1987**.

[3] J. J. Rehr, R. C. Albers, *Rev. Mod. Phys.* **2000**, *72*, 621.

[4] a) G. Kresse, J. Furthmu¨ller, *Phys. Rev. B* **1996**, *54*, 11169; b) G. Kresse, J. Furthmiiller, *Comput. Mater. Sci.* **1996**, *6*, 15-50.

[5] G. Kresse, D. Joubert, *Phys. Rev. B* **1999**, *59*, 1758.

[6] J. P. Perdew, K. Burke, E. M, *Phys. Rev. Lett.* **1996**, *77*, 3765.

[7] S. Grimme, J. Antony, S. Ehrlich, H. Krieg, *J. Chem. Phys.* **2010**, *132*, 154104.

[8] W. Setyawan, S. Curtarolo, *Comput. Mater. Sci.* **2010**, *49*, 299-312.

[9] V. Wang, N. Xu, J.-C. Liu, G. Tang, W.-T. Geng, *Comput. Phys. Commun.* **2021**, *267*.

[10] D. Zhao, K. Sun, W. C. Cheong, L. Zheng, C. Zhang, S. Liu, X. Cao, K. Wu, Y. Pan, Z. Zhuang, B. Hu, D. Wang, Q. Peng, C. Chen, Y. Li, *Angew. Chem. Int. Ed. Engl.* **2020**, *59*, 8982-8990.

[11] T. J. M. M. H. V. Huynh, *Chem. Rev.* **2007**, *107*, 5004−5064.

[12] a) J. K. Norskov, F. Abild-Pedersen, F. Studt, T. Bligaard, *PNAS* **2011**, *108*, 937-943; b) S. J. Hwang, S. K. Kim, J. G. Lee, S. C. Lee, J. H. Jang, P. Kim, T. H. Lim, Y. E. Sung, S. J. Yoo, *J. Am. Chem. Soc.* **2012**, *134*, 19508-19511.

[13] K. Momma, F. Izumi, *J. Appl. Crystallogr.* **2008**, *41*, 653-658.

[14] X. Zheng, J. Xu, K. Yan, H. Wang, Z. Wang, S. Yang, *Chem. Mater.* **2014**, *26*, 2344-2353.

[15] Y. Ito, W. Cong, T. Fujita, Z. Tang, M. Chen, *Angew. Chem. Int. Ed.* **2015**, *54*, 2131-2136.

[16] H. Yan, C. Tian, L. Wang, A. Wu, M. Meng, L. Zhao, H. Fu, *Angew. Chem. Int. Ed.* **2015**, *54*, 6325-6329.

[17] J. Duan, S. Chen, B. A. Chambers, G. G. Andersson, S. Z. Qiao, *Adv. Mater.* **2015**, *27*, 4234-4241.

[18] Y. Teng, X. D. Wang, H. Y. Chen, J. F. Liao, W. G. Li, D. B. Kuang, *J. Mater. Chem. A* **2017**, *5*, 22790–22796.

[19] M. Lin, R. Lu, W. Luo, N. Xu, Y. Zhao, L. Mai, *ACS Applied Energy Materials* **2021**, *4*, 5486-5492.

[20] P. Xiao, M. Alam Sk, L. Thia, X. M. Ge, R. J. Lim, J. Y. Wang, K. H. Lim, X. Wang, *Energy Environ. Sci.* **2014**, *7*, 2624-2629.

[21] J. Yang, F. Zhang, X. Wang, D. He, G. Wu, Q. Yang, X. Hong, Y. Wu, Y. Li, *Angew. Chem. Int. Ed.* **2016**, *55*, 12854-12858.

[22] X. Zhang, X. Yu, L. Zhang, F. Zhou, Y. Liang, R. Wang, *Adv. Funct. Mater.* **2018**, 1706523.

[23] H. Yan, Y. Jiao, A. Wu, C. Tian, X. Zhang, L. Wang, Z. Ren, H. Fu, *Chem. Commun.* **2016**, *52*, 9530-9533.

[24] X. Chen, D. Wang, Z. Wang, P. Zhou, Z. Wu, F. Jiang, *Chem. Commun.* **2014**, *50*, 11683-11685.

[25] T. Y. Wang, K. Z. Du, W. L. Liu, Z. W. Zhu, Y. H. Shao, M. X. Li, *J. Mater. Chem. A* **2015**, *3*, 4368–4373.

[26] Z. Pu, I. S. Amiinu, X. Liu, M. Wang, S. Mu, *Nanoscale* **2016**, *8*, 17256-17261.

[27] K. Ojha, M. Sharma, H. Kolev, A. K. Ganguli, *Catal. Sci. Technol.* **2017**, *7*, 668-676.

[28] Z. Xing, Q. Liu, A. M. Asiri, X. Sun, *Adv. Mater.* **2014**, *26*, 5702-5707.

[29] A. Wu, C. Tian, H. Yan, Y. Jiao, Q. Yan, G. Yang, H. Fu, *Nanoscale* **2016**, *8*, 11052-11059.

[30] Q. Zhou, J. Feng, X. Peng, L. Zhong, R. Sun, *Journal of Energy Chemistry* **2020**, *45*, 45-51.

[31] R. Ye, P. del Angel-Vicente, Y. Liu, M. J. Arellano-Jimenez, Z. Peng, T. Wang, Y. Li, B. I. Yakobson, S. H. Wei, M. J. Yacaman, *Adv. Mater.* **2015**.

[32] Z. Pu, I. Saana Amiinu, M. Wang, Y. Yang, S. Mu, *Nanoscale* **2016**, *8*, 8500-8504.

[33] Y. Huang, J. X. Ge, J. Hu, J. W. Zhang, J. Hao, Y. G. Wei, *Adv. Energy Mater.* **2018**, *8*, 1701601.

[34] S. J. Aravind, K. Ramanujachary, A. Mugweru, T. D. Vaden, *Applied Catalysis A: General* **2015**, *490*, 101-107.